

Micron-Scale Deformation: A Coupled *In Situ* Study of Strain Bursts and Acoustic Emission

Ádám István Hegyi,¹ Péter Dusán Ispánovity,^{1,*} Michal Knapek,² Dániel Tüzes,¹ Kristián Máthis,² František Chmelík,² Zoltán Dankházi,¹ Gábor Varga,¹ and István Groma¹

¹Department of Materials Physics, Eötvös Loránd University, Pázmány Péter sétány 1/a, H-1117 Budapest, Hungary

²Faculty of Mathematics and Physics, Department of Physics of Materials, Charles University in Prague, Ke Karlovu 5, 121 16 Prague 2, Czech Republic

Abstract: Plastic deformation of micron-scale crystalline materials differs considerably from bulk samples as it is characterized by stochastic strain bursts. To obtain a detailed picture of the intermittent deformation phenomena, numerous micron-sized specimens must be fabricated and tested. An improved focused ion beam fabrication method is proposed to prepare non-tapered micropillars with excellent control over their shape. Moreover, the fabrication time is less compared with other methods. The *in situ* compression device developed in our laboratory allows high-accuracy sample positioning and force/displacement measurements with high data sampling rates. The collective avalanche-like motion of the dislocations is observed as stress decreases on the stress–strain curves. An acoustic emission (AE) technique was employed for the first time to study the deformation behavior of micropillars. The AE technique provides important additional *in situ* information about the underlying processes during plastic deformation and is especially sensitive to the collective avalanche-like motion of the dislocations observed as the stress decreases on the deformation curves.

Key words: micropillar compression, *in situ* deformation, acoustic emission, microsample fabrication

INTRODUCTION

In the past decades, the miniaturization of mechanical and electronic devices has inspired research to determine the mechanical properties of micron-sized specimens (Volkert & Lilleodden, 2006; Ng & Ngan, 2008; Zaiser et al., 2008; Kraft et al., 2010; Zhou et al., 2011). Many microelectromechanical devices (e.g., micromachined inertial sensors or cantilever transducer platforms for chemical and biological sensors) contain micrometer-sized components (Yazdi et al., 1998; Lavrik et al., 2004). To design progressively smaller devices, the detailed physical events underlying the deformation processes in the microparts must be understood.

Plastic deformation of crystalline materials typically occurs by the collective motion of dislocation ensembles. The stress–strain response of macroscopic samples is generally smooth and reproducible due to the large number of moving dislocations, thus allowing highly accurate predictions of the material properties. In contrast, at micrometer scales, the inhomogeneities in the dislocation structure can be on the order of the sample size, leading to a discontinuous response due to the stochastic activation of dislocation avalanches (Miguel et al., 2002; Weiss & Marsan, 2003; Zaiser et al., 2004; Zaiser & Moretti, 2005; Zapperi, 2012). Therefore, a statistical approach must be employed to assess the mechanical behavior of materials at this scale.

The initial evidence of intermittent crystal plasticity was observed in single ice crystals by detecting strong acoustic

emission (AE) signals during creep deformation (Weiss et al., 2000; Miguel et al., 2001). A decade ago, Dimiduk et al. found that instabilities in the form of strain jumps dominate micrometer-scale crystal plasticity by compressing pure single-crystalline Ni micropillars (Uchic et al., 2004; Dimiduk et al., 2006; Uchic et al., 2009), raising the questions (i) where is the limit between microscopic and macroscopic deformation, and (ii) how can material strength parameters, such as yield point or ultimate compressive/tensile strength, be defined for micron-scale objects (Arzt, 1998; Greer & De Hosson, 2011; Ispánovity et al., 2013).

Due to their statistical nature, revealing the properties of microdeformation requires numerous samples to be tested. One of the most typical and frequently applied methods for fabricating microsamples (micropillars) is focused ion beam (FIB) milling (Reyntjens & Puers, 2001). The main advantage of this method is the ability to continuously visually control the fabrication process. Moreover, there is practically no limitation on the materials from which the micropillars can be milled. Conversely, FIB-based methods are rather time consuming. To shorten the fabrication time of micropillars, several different (FIB-less) methods are being developed (Burek & Greer, 2009; Jennings et al., 2010). Unfortunately, FIB-less methods typically do not allow the production of pillars from any type of material. Furthermore, the initial dislocation density of the samples can be difficult to control, or the connecting force between the substrate and the grown micropillars can be rather weak (Moser et al., 2012).

Two approaches are commonly applied to fabricate micropillars by FIB milling: “lathe” and “annular” milling

Received October 21, 2016; accepted August 29, 2017

*Corresponding author. ispanovity@metal.elte.hu

(Hütsch & Lilleodden, 2014). Lathe milling uses an ion beam (almost) perpendicular to the axis of the micropillar. The substrate is rotated during milling, resulting in a cylindrical micropillar. Conversely, in annular milling, the pillar axis is parallel to the ion beam and the ions etch the surface of the substrate. Both methods have advantages and disadvantages. Lathe milling provides perfect control over the final geometry of the sample; however, there are significant effects from ion implantation on the mechanical properties of the micropillars. The annular method always produces tapered micropillars and the height is only loosely controlled. However, the annular method is considerably faster and the negative effects of ion damage are much weaker (Hütsch & Lilleodden, 2014). The new method outlined here combines the advantages of both techniques. With this procedure, non-tapered micropillars can be milled anywhere on the surface of a bulk material, with well-defined geometry and preparation times comparable with the annular method (Wurster et al., 2015).

The long-term goal is to determine the fundamentals of plastic deformation at the micrometer scale. The new micropillar fabrication procedure presented in this work enables us to produce a high number of samples in a shorter time. This, in turn, allows for good statistical analysis of the erratic deformation behavior of micropillars arising from the stochastic response of dislocation ensembles to the acting force (Miguel et al., 2001, 2002; Dimiduk et al., 2006; Zaiser, 2006; Ispánovity et al., 2010). Thus, even though a single measurement cannot provide important material parameters, this information can be derived from extensive systematic testing (Ispánovity et al., 2010, 2013).

Introductory compression tests were performed on Al-5% Mg alloy micropillars fabricated onto the surface of the bulk material. Importantly, this alloy exhibits the Portevin–Le Chatelier (PLC) effect (Tabata et al., 1980; Chinh et al., 2000; Gubicza et al., 2004; Yilmaz, 2011). In this type of bulk sample, the intermittent stress–strain response originates in the repeated pile-ups and break-outs (pinning and unpinning) of dislocations from the atmosphere of solute atoms where these atoms act as obstacles for mobile dislocations (Gubicza et al., 2004; Yilmaz, 2011). This mechanism generates strong acoustic signals with typically greater energies than those caused by non-PLC dislocation avalanches during plastic deformation. As the stress drops caused by the PLC effect and dislocation avalanches lead to a measurable AE, the tests on this material allowed us to verify the sensitivity of our AE detection system.

SAMPLE PREPARATION

Before fabrication, the geometry and size of the micropillar must be decided. As this study focuses on collective dislocation phenomena, samples with high initial dislocation density are required. At the same time, the sample size should not be too large, which would lead to bulk deformation, thus hindering the occurrence of clearly distinguishable stress drops. Normally, in fcc metals such as Al, the

dislocation density varies between 10^{11} and 10^{14} m^{-2} . Therefore, it can be derived that the average spacing between dislocations is $\sim 0.1\text{--}3 \mu\text{m}$. As the dislocations tend to form cell-like structures with a characteristic size of approximately 10 times the dislocation spacing, the pillar size is selected to be on the order of the cell size. It should be noted that in deformed micropillars the cell size may also depend on the sample size; nevertheless, the cell size-to-dislocation spacing ratio remains ~ 10 (Yu et al., 2014; El-Awady, 2015).

In situ micropillar deformation tests demand very careful and precise sample preparation. To obtain the required surface properties, orientation, and initial dislocation density, the following steps were performed. After a short etching, the Al-5% Mg bulk substrate was electropolished in perchloric electrolyte D2 solution with a 60 mA/mm^2 current density. The lattice orientation was measured using electron backscatter diffraction (EBSD). The sample was cut with an electric discharge machine to have the normal surface oriented parallel to the $\langle 123 \rangle$ direction. Next, further electropolishing was performed, followed by a heat treatment for 72 h at 200°C . Finally, the surface was electropolished again with a 30 mA/mm^2 current density, and the orientation was checked again with EBSD. The sample was predeformed along the $\langle 123 \rangle$ direction with a load of 20 MPa. An initial dislocation density of $2 \times 10^{13} \text{ m}^{-2}$ was measured with transmission electron microscope and X-ray line profile analysis. With this value, a pillar geometry with a rectangular cross-section of $4 \times 4 \mu\text{m}^2$ and a height of $12 \mu\text{m}$ was selected, corresponding to an aspect ratio of 3:1:1, which was commonly applied in earlier studies.

After the abovementioned sample preparation processes, a “surrounding hole” was milled by a 30 nA ion current around the micropillar. The FIB milling pattern is marked by the grid in Figure 1a. The sample was oriented so that the normal vector of the surface was parallel to the ion beam direction. A thin Pt layer was then deposited onto the top surface of the micropillar. The cap ensures the ion beam will fabricate a smooth side surface on the pillar. Moreover, due to its amorphous structure, the cap is very hard; hence it helps (eliminate the effects related to a possible misalignment between the surfaces of the compressing tip and the sample during the compression test. Therefore, the stress becomes more homogeneous below the Pt layer than at the contact between the tip and the sample surface. Next, the stage is tilted by 7° . In combination with the 52° ion–electron beam angle, this results in a 45° ion beam direction with respect to the surface normal. To ensure precise and easy positioning of the scanning electron microscope (SEM) stage, a small cross ($2 \mu\text{m}$) was imprinted onto the geometric center of the top surface of the micropillar. Afterwards, the individual milling steps were performed. These steps are explained in detail in Figure 2. To further decrease tapering (Li et al., 2006), a final “polishing” step was performed with 100 pA ion beam over-tilted by 1° with respect to the pillar axis (normal to the top surface of the pillar).

Apart from the first step explained above, the entire fabrication is performed with high milling angles.

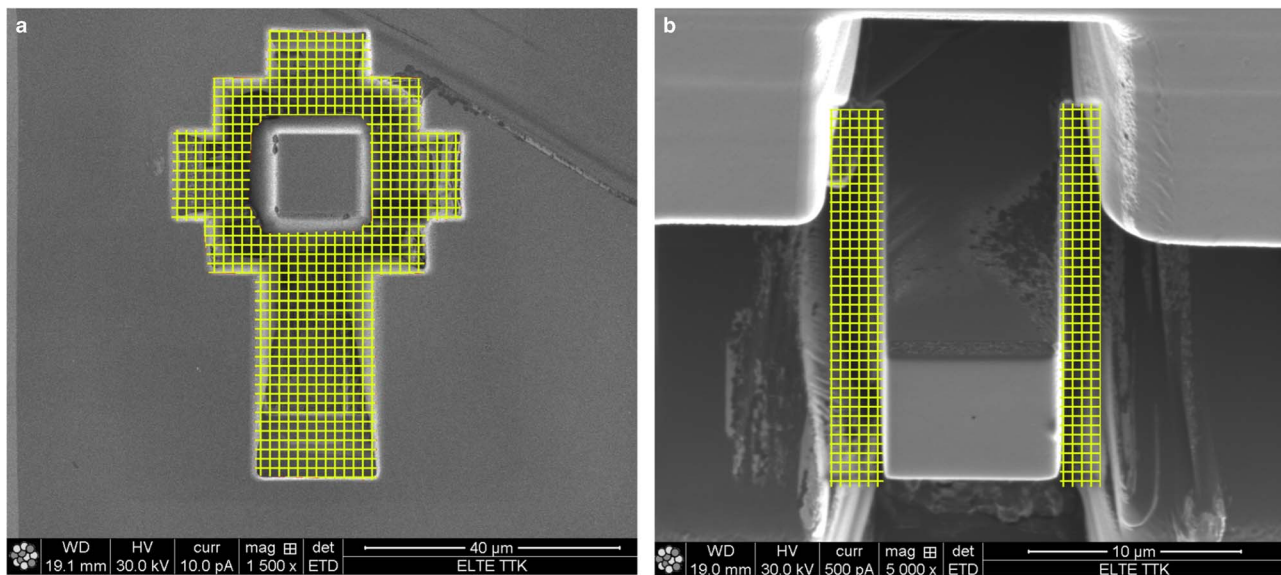


Figure 1. **a:** The initial focused ion beam milling step (marked by the grid) to fabricate the “raw” pillar and the hole around it. A large enough hole is necessary for the compression test. For this milling step, a 30-nA ion current is applied. **b:** The second and final milling step uses a 45° ion direction angle (see Fig. 2). The ion current is 5 nA, and the area removed during this step is marked by the grid. Both pictures are taken from the ion direction.

This increases the effectiveness of the milling by a factor of 2.5–3 compared with the commonly used perpendicular beam setup (Ishitani et al., 2004). The 45° milling direction applied in the second phase allows for the fabrication of micropillars anywhere on the flat sample surface. Recall that the Ga ion beam forms an irradiated layer on the micropillar. However, the slightly tilted final polishing step with the reduced 100 pA ion current and lowered acceleration voltage (20 kV or 10 kV) significantly diminishes the deteriorating effect of ion implantation in the studied pillar sizes (Greer et al., 2008).

To sum up, the most important features of the proposed milling procedure are as follows: (i) micropillars can be fabricated at any position on the substrate surface, (ii) preparation is touchless, thus damage or predeformation of the pillar can be avoided during the entire production process, (iii) the final pillar is practically taper-free (the inclination of the side surface was always less than $\pm 0.5^\circ$), (iv) the method is relatively fast, with an average milling time of < 4 h for a $4 \times 4 \times 12 \mu\text{m}^3$ pillar (the fabrication time is similar to the average milling times using the annular method for the same pillar size), and (v) detrimental effects related to Ga implantation can be suppressed.

IN SITU DEVICE

An *in situ* micromechanical test requires that the testing device be placed inside the chamber of the SEM. Such a compression device was developed in our laboratory for implementation in an FEI Quanta 3D SEM (FEI, Hillsboro, OR, USA). A schematic of the device is shown in Figure 3.

Two linear ultrasonic motors position the sample in the X and Y directions. The AE transducer is mounted on the top of this double stage. In the Z direction, two stages are used.

One is a linear step-motor stage for “raw” movement of the compressing tip closer to the sample. The second stage, mounted on the linear step-motor stage, is a piezoelectric positioning (PEP) stage with a resolution of ~ 0.1 nm. During the compression test, only this stage is moved. A standard spring mounted on the PEP stage, with high transversal but very low longitudinal stiffness, is used to measure the external force. The elongation e of the spring is measured by a capacitive sensor with 0.1 nm resolution. If the PEP stage is moved a distance d , and the capacitive sensor measures an elongation e , then the sample deformation is $\epsilon = d - e$, and the acting force is $F = ke$, where k is the stiffness of the spring. Pillar compression is performed with a flat punch diamond tip. To avoid charging the compressing head in the SEM, a boron-doped tip must be used.

To measure instabilities related to the PLC effect and dislocation avalanches, a fast feedback controlling system and a minimum data collection rate of 1 kHz are crucial. This is achieved by analogous proportional–integral–derivative-type feedback electronics and a fast 16 bit AD converter. The range and resolution parameters of the device are summarized in Table 1.

To achieve the listed resolutions, the thermal and elastic elongation of the device components must remain negligible during the entire measurement (typically several minutes). For this reason, several additional parts were added to the compression device. The main issue was reducing the heat produced by the stage motors. Therefore, the Quanta 3D SEM is equipped with an environmental stage with a Peltier sample holder to control the sample temperature. The cold point of the Peltier stage is mounted to the bottom of the device, stabilizing the temperature at 15°C. Another issue was the vibrations of the force sensor spring due to the absence of the damping effect of air in the evacuated

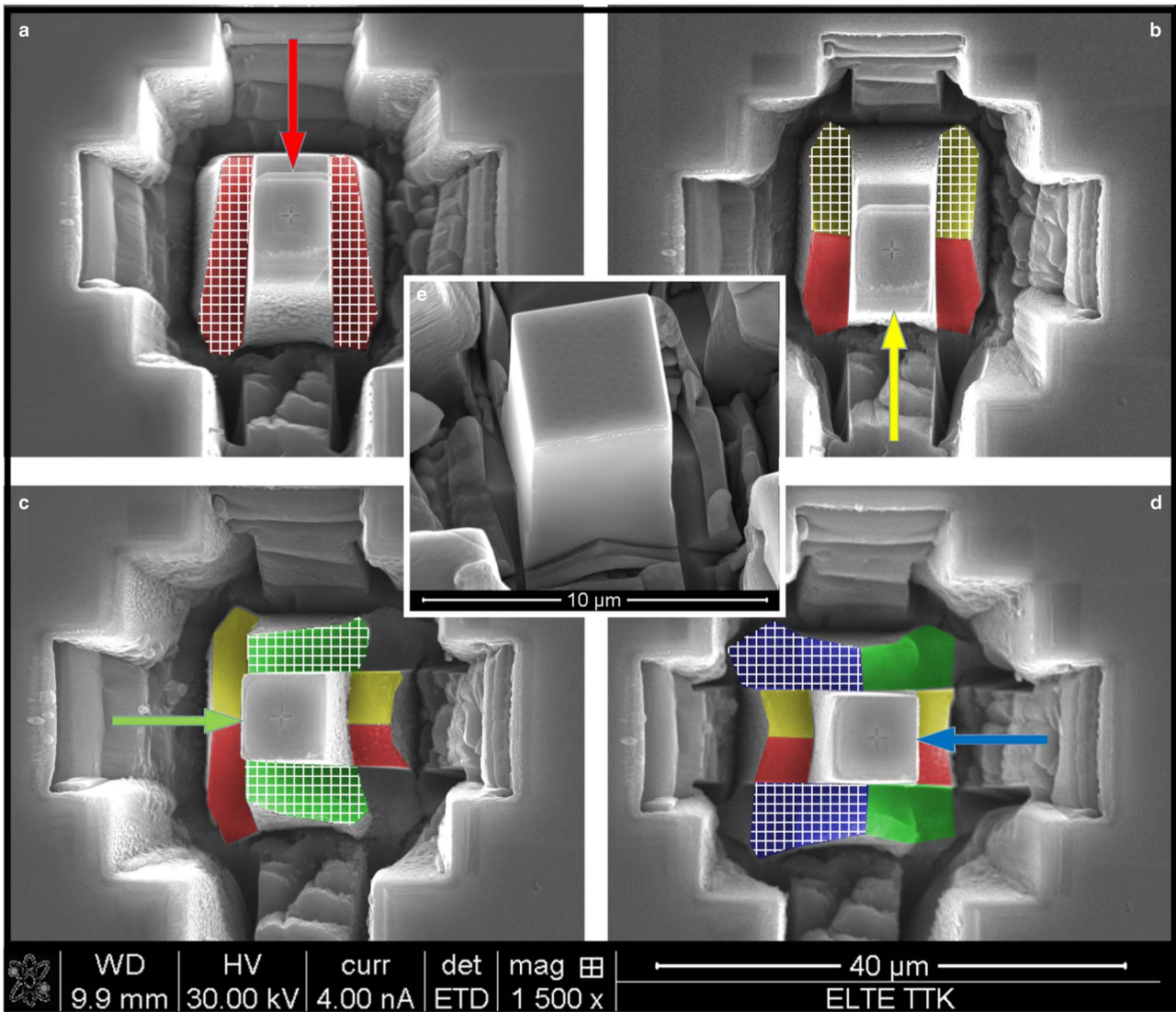


Figure 2. Detail of the second, final step of the micropillar fabrication procedure with an ion current of 5 nA. **a:** After the first step, described in Figure 1, the sample is tilted by 45° resulting in a tilted ion beam direction. Then, two rectangular focused ion beam (FIB) patterns are used to obtain the surface marked in red. **b:** Next, the sample is rotated by 180° and the two rectangular FIB patterns are used again for the surface marked in yellow. By rotating 90° and repeating the previous two steps, the surfaces marked by (c) green and (d) blue are obtained. Finally, a rectangular-shaped pillar is obtained. To craft a pillar with smooth surfaces and practically no tapering, the entire procedure is repeated with ion currents of 1 nA and 100 pA. The final pillar is shown in the inset (e).

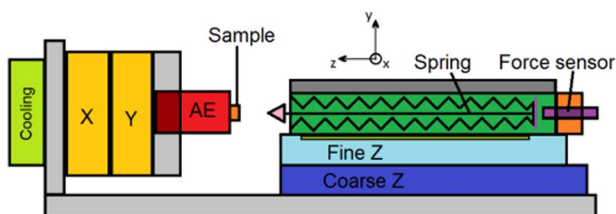


Figure 3. Schematic view of the *in situ* device for the NanoTest. AE, acoustic emission.

chamber. To suppress this disturbing effect, strong permanent magnets were placed near the lamellae of the force measuring spring, thus providing the necessary damping from the eddy currents.

AE MEASUREMENTS

An AE measuring system was employed to study the dynamic processes during the plastic deformation of micropillars. AEs are transient elastic waves generated by the rapid release of energy from localized sources within the material. Therefore, AE signals can be detected when sudden localized structural changes, such as collective dislocation motion or twinning, occur. Consequently, the AE technique provides information about the dynamic phenomena involved in plastic deformation (Heiple & Carpenter, 1987).

In bulk materials, a direct correlation of the AE parameters with the stress–strain curves reveals the activation of different deformation mechanisms (Bohlen et al., 2004;

Table 1. Main Parameters of the NanoTest device.

| Part name | Total range | Resolution | Accuracy |
|--|------------------|---------------------|---------------------|
| X and Y stages | ± 8 mm | $0.5 \mu\text{m}$ | $0.01 \mu\text{m}$ |
| Coarse Z stage | 9 mm | $2 \mu\text{m}$ | $0.5 \mu\text{m}$ |
| Fine Z stage | $35 \mu\text{m}$ | 1 nm | 0.1 nm |
| Force sensor (with two possible presets) | 20/50 mN | $1/2.5 \mu\text{N}$ | $1/2.5 \mu\text{N}$ |

Weiss et al., 2007; Dobroň et al., 2009; Kovacs et al., 2014). The collective motion of several tens or hundreds of dislocations is necessary to obtain a detectable AE signal (Scruby et al., 1981). Thus, in terms of AE, the motion of a single dislocation is typically “silent” and a detectable AE signal (if caused by dislocation activity) reflects cooperative dislocation motion.

Crackling or avalanche-like plasticity is not only characteristic for micron-scale objects but also for bulk samples (Weiss et al., 2007). Due to the enormous number of moving dislocations in macroscopic samples, averaging occurs, which results in a smooth and seemingly continuous stress–strain dependence. Conversely, the AE technique may provide valuable information about underlying dynamic processes that cannot be derived from deformation curves. To our knowledge, this study is the first attempt to record AE signals during mechanical tests on microsamples.

AE signal measurements were performed with a Physical Acoustics PCI-2 acquisition board based on the continuous storage of AE signals with a 2 MHz sampling rate. The full scale of the A/D converter was ± 10 V. The AE signal was preamplified by 60 dB for frequencies from 100 – 1,200 kHz. The background noise did not exceed 24 dB and the detecting threshold level was 26 dB. AE was recorded simultaneously with load–strain data during the uniaxial compression of the micropillar. A rectangular piece of material (with micropillar

samples fabricated onto its surface) was attached directly to the AE transducer using a metallic spring. In addition, the acoustic contact was improved with vacuum grease.

Load as a function of time and the AE signal recorded during the test of the Al-5% Mg micropillar at a constant compressive strain rate are plotted in Figure 4. As expected, the sample exhibits the well-known PLC effect. We speculate that the stress drops at the very beginning of deformation and just before plastic yielding [enlarged in inset (a)] correspond to the break-out of dislocations from the surrounding solute atoms. The stress drops between these two drops are much smaller, but definitely above the noise level of the instrument. Therefore, they may correspond to dislocation avalanches. Further investigations are required to assess how PLC-type stress drops differ from dislocation avalanches, for example, in non-PLC pure Al micropillars. As seen in inset (a), a large AE signal is detected at the onset of the stress drop. For the micropillar dimensions used, $4 \times 4 \times 12 \mu\text{m}^3$, the PLC effect can compete with intrinsic intermittent dislocation motion (dislocation avalanches). The combined effect conceals the well-known periodic stress drop structure of the deformation curve, and randomly distributed avalanches are observed. In inset (b), the waveform of the acoustic signal displays several large peaks.

SUMMARY

To understand in detail the deformation properties of micron-sized samples, experiments performed on large ensembles of specimens are needed. The micropillar fabrication method presented is considerably faster than previous methods. This introduces the possibility of investigations that can reveal the statistical properties of micron-scale plasticity. The results further indicate that the detection of an AE signal related to the cooperative motion of dislocations is feasible even for microscopic samples with small volumes of $\sim 100 \mu\text{m}^2$.

ACKNOWLEDGMENTS

P.D.I. and I.G. acknowledge financial supports from the National Research, Development and Innovation Found of Hungary under the project Nos. NKFIH-K-119561 and NKFIH-PD-105256. P.D.I. is also supported by the Janos Bolyai Scholarship of the Hungarian Academy of Sciences and by the European Commission under grant agreement No. CIG-321842. P.D.I., M.K., K.M., and F.C. are grateful for the financial support from the Czech Science Foundation under contract 15-10821S.

REFERENCES

- ARZT, E. (1998). Size effects in materials due to microstructural and dimensional constraints: A comparative review. *Acta Mater* **46**(16), 5611–5626.
- BOHLEN, J., CHMELÍK, F., DOBROŇ, P., LETZIG, D., LUKÁČ, P. & KAINER, K. (2004). Acoustic emission during tensile testing of magnesium AZ alloys. *J Alloys Compd* **378**(1), 214–219.

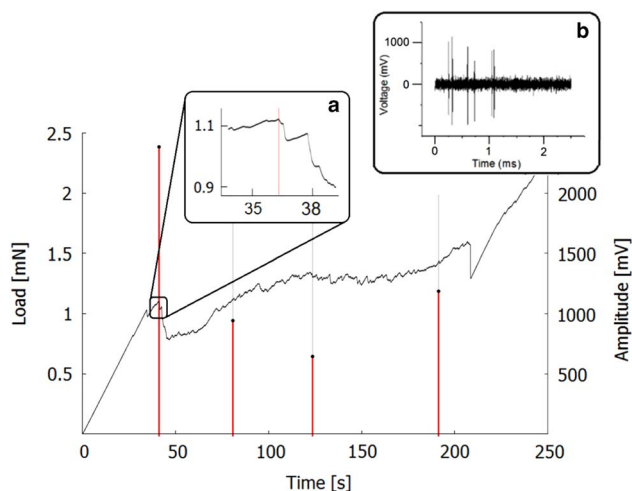


Figure 4. Load versus time curve obtained from a micropillar compression test at a constant strain rate. In inset (a), a stress drop is enlarged. Inset (b) shows the waveform of an individual acoustic emission peak.

- BUREK, M.J. & GREER, J.R. (2009). Fabrication and microstructure control of nanoscale mechanical testing specimens via electron beam lithography and electroplating. *Nano Lett* **10**(1), 69–76.
- CHINH, N., CSIKOR, F., KOVÁCS, Z. & LENDVAI, J. (2000). Critical concentration of Mg addition for plastic instabilities in Al–Mg alloys. *J Mater Res* **15**(5), 1037–1040.
- DIMIDUK, D.M., WOODWARD, C., LESAR, R. & UCHIC, M.D. (2006). Scale-free intermittent flow in crystal plasticity. *Science* **312**(5777), 1188–1190.
- DOBROŃ, P., CHMELIK, F., BOHLEN, J., HANTZSCHE, K., LETZIG, D. & ULRICH KAINER, K. (2009). Acoustic emission study of the mechanical anisotropy of the extruded AZ31 alloy. *Int J Mater Res* **100**(6), 888–891.
- EL-AWADY, J.A. (2015). Unravelling the physics of size-dependent dislocation-mediated plasticity. *Nat Commun* **6**, 5926.
- GREER, J.R. & DE HOSSON, J.T.M. (2011). Plasticity in small-sized metallic systems: Intrinsic versus extrinsic size effect. *Prog Mater Sci* **56**(6), 654–724.
- GREER, J.R., ESPINOSA, H., RAMESH, K. & NADGORNÝ, E. (2008). Comment on “effects of focused ion beam milling on the nanomechanical behavior of a molybdenum-alloy single crystal”. *Appl Phys Lett* **92**(9), 096101.
- GUBICZA, J., CHINH, N.Q., HORITA, Z. & LANGDON, T. (2004). Effect of Mg addition on microstructure and mechanical properties of aluminum. *Mater Sci Eng A* **387**, 55–59.
- HEIPLE, C. & CARPENTER, S. (1987). Acoustic emission from low temperature phase transformations in plutonium. *J Nucl Mater* **149**(2), 168–179.
- HÜTSCH, J. & LILLEODDEN, E.T. (2014). The influence of focused-ion beam preparation technique on microcompression investigations: Lathe vs. annular milling. *Scr Mater* **77**, 49–51.
- ISHITANI, T., UMEMURA, K., OHNISHI, T., YAGUCHI, T. & KAMINO, T. (2004). Improvements in performance of focused ion beam cross-sectioning: Aspects of ion-sample interaction. *J Electron Microsc* **53**(5), 443–449.
- ISPÁNOVITY, P.D., GROMA, I., GYÖRGYI, G., CSIKOR, F.F. & WEYGAND, D. (2010). Submicron plasticity: Yield stress, dislocation avalanches, and velocity distribution. *Phys Rev Lett* **105**(8), 085503.
- ISPÁNOVITY, P.D., HEGYI, Á., GROMA, I., GYÖRGYI, G., RATTER, K. & WEYGAND, D. (2013). Average yielding and weakest link statistics in micron-scale plasticity. *Acta Mater* **61**(16), 6234–6245.
- JENNINGS, A.T., BUREK, M.J. & GREER, J.R. (2010). Microstructure versus size: Mechanical properties of electroplated single crystalline Cu nanopillars. *Phys Rev Lett* **104**(13), 135503.
- KOVÁCS, Z., EZZELDIEN, M., MÁTHIS, K., ISPÁNOVITY, P., CHMELIK, F. & LENDVAI, J. (2014). Statistical analysis of acoustic emission events in torsional deformation of a vitreous bulk metallic glass. *Acta Mater* **70**, 113–122.
- KRAFT, O., GRUBER, P.A., MÖNIG, R. & WEYGAND, D. (2010). Plasticity in confined dimensions. *Ann Rev Mater Res* **40**, 293–317.
- LAVRIK, N.V., SEPANIÁK, M.J. & DATSKOS, P.G. (2004). Cantilever transducers as a platform for chemical and biological sensors. *Rev Sci Instrum* **75**(7), 2229–2253.
- LI, J., MALIS, T. & DIONNE, S. (2006). Recent advances in FIB–TEM specimen preparation techniques. *Mater Character* **57**(1), 64–70.
- MIGUEL, M.-C., VESPIGNANI, A., ZAISER, M. & ZAPPERI, S. (2002). Dislocation jamming and Andrade creep. *Phys Rev Lett* **89**(16), 165501.
- MIGUEL, M.-C., VESPIGNANI, A., ZAPPERI, S., WEISS, J. & GRASSO, J.-R. (2001). Intermittent dislocation flow in viscoplastic deformation. *Nature* **410**(6829), 667–671.
- MOSER, G., FELBER, H., RASHKOVA, B., IMRICH, P., KIRCHLECHNER, C., GROSINGER, W., MOTZ, C., DEHM, G. & KIENER, D. (2012). Sample preparation by metallography and focused ion beam for nanomechanical testing. *Pract Metallogr* **49**(6), 343–355.
- NG, K. & NGAN, A. (2008). Stochastic nature of plasticity of aluminum micro-pillars. *Acta Mater* **56**(8), 1712–1720.
- REYNTJENS, S. & PUERS, R. (2001). A review of focused ion beam applications in microsystem technology. *J Micromech Microeng* **11**(4), 287.
- SCRUBY, C., WADLEY, H., RUSBRIDGE, K. & STOCKHAM-JONES, D. (1981). Influence of microstructure on acoustic emission during deformation of aluminium alloys. *Metal Sci* **15**(11–12), 599–608.
- TABATA, T., FUJITA, H. & NAKAJIMA, Y. (1980). Behavior of dislocations in Al–Mg single crystals observed by high voltage electron microscopy. *Acta Metall* **28**(6), 795–805.
- UCHIC, M.D., DIMIDUK, D.M., FLORANDO, J.N. & NIX, W.D. (2004). Sample dimensions influence strength and crystal plasticity. *Science* **305**(5686), 986–989.
- UCHIC, M.D., SHADE, P.A. & DIMIDUK, D.M. (2009). Plasticity of micrometer-scale single crystals in compression. *Ann Rev Mater Res* **39**, 361–386.
- VOLKERT, C.A. & LILLEODDEN, E.T. (2006). Size effects in the deformation of sub-micron Au columns. *Philos Mag* **86**(33–35), 5567–5579.
- WEISS, J., LAHAIE, F. & GRASSO, J.R. (2000). Statistical analysis of dislocation dynamics during viscoplastic deformation from acoustic emission. *J Geophys Res Solid Earth* **105**(B1), 433–442.
- WEISS, J. & MARSAN, D. (2003). Three-dimensional mapping of dislocation avalanches: Clustering and space/time coupling. *Science* **299**(5603), 89–92.
- WEISS, J., RICHETON, T., LOUCHET, F., CHMELIK, F., DOBRON, P., ENTEMEYER, D., LEBYODKIN, M., LEBEDKINA, T., FRESSENGEAS, C. & McDONALD, R.J. (2007). Evidence for universal intermittent crystal plasticity from acoustic emission and high-resolution extensometry experiments. *Phys Rev B* **76**(22), 224110.
- WURSTER, S., TREML, R., FRITZ, R., KAPP, M., LANGS, E., ALFREIDER, M., RUHS, C., IMRICH, P., FELBER, G. & KIENER, D. (2015). Novel methods for the site specific preparation of micromechanical structures: Presented at the metallography conference 2014 in Leoben, Austria. *Pract Metallogr* **52**(3), 131–146.
- YAZDI, N., AYAZI, F. & NAJAFI, K. (1998). Micromachined inertial sensors. *Proc IEEE* **86**(8), 1640–1659.
- YILMAZ, A. (2011). The Portevin–Le Chatelier effect: A review of experimental findings. *Sci Technol Adv Mater* **12**, 063001.
- YU, Q., MISHRA, R.K., MORRIS, J.W. Jr. & MINOR, A.M. (2014). The effect of size on dislocation cell formation and strain hardening in aluminium. *Philos Mag* **94**(18), 2062–2071.
- ZAISER, M. (2006). Scale invariance in plastic flow of crystalline solids. *Adv Phys* **55**(1–2), 185–245.
- ZAISER, M., GRASSET, F.M., KOUTSOS, V. & AIFANTIS, E.C. (2004). Self-affine surface morphology of plastically deformed metals. *Phys Rev Lett* **93**(19), 195507.
- ZAISER, M. & MORETTI, P. (2005). Fluctuation phenomena in crystal plasticity—A continuum model. *J Stat Mech* **2005**(8), P08004.
- ZAISER, M., SCHWERTFEGGER, J., SCHNEIDER, A., FRICK, C., CLARK, B.G., GRUBER, P. & ARZT, E. (2008). Strain bursts in plastically deforming molybdenum micro- and nanopillars. *Philos Mag* **88**(30–32), 3861–3874.
- ZAPPERI, S. (2012). Current challenges for statistical physics in fracture and plasticity. *Eur Phys J B* **85**(9), 1–12.
- ZHOU, C., BEYERLEIN, I.J. & LESAR, R. (2011). Plastic deformation mechanisms of fcc single crystals at small scales. *Acta Mater* **59**(20), 7673–7682.